



DLC-Coated Thermoplastics: Tribological Analyses Under Dry and Lubricated Sliding Conditions

K. Bobzin¹ · C. Kalscheuer¹ · M. Thiex¹ · P. Sperka² · M. Hartl² · S. Reitschuster³ · E. Maier³ · T. Lohner³ · K. Stahl³

Received: 20 July 2022 / Accepted: 2 October 2022 / Published online: 23 November 2022
© The Author(s) 2022

Abstract

The purpose of this study was to increase the limited wear resistance of polymers in highly stressed tribological contacts. Therefore, diamond-like carbon (DLC) coatings were firstly developed and deposited on polymers. The development of the low temperature coating process was conducted on an industrial scale coating unit. Due to the use of polyether ether ether ketone (PEEK) and polyamide as substrate material, the coatings were tailored in accordance with different mechanical properties of the polymers. Furthermore, analyses regarding morphology, roughness as well as compound adhesion between coatings and polymers were conducted. The tribological analyses were accomplished for reciprocating sliding kinematics on pin-on-plate tribometer under dry conditions as well as boundary lubricated conditions. The results prove the ability of the coatings to undergo high plastic deformations without delamination. In addition, the possible formation of a composite layer of DLC and PEEK in the wear track due to high energy input under dry conditions was shown. Furthermore, the transformations of sp^2 chain into ring bindings as well as a change of size and distribution of the sp^2 clusters during dry contact conditions were observed.

Keywords DLC · PEEK · PA66 · Raman spectroscopy · Wear · Polymers

1 Introduction

Nowadays, the mechanical engineering sector needs to meet increasing demands on products in terms of lightweight construction, cost efficiency and performance under the prerequisite of saving resources. In order to meet these requirements, the substitution of metallic materials with polymers is a target-oriented approach. A typical representative of a substitute is poly ether ether ketone (PEEK), which has been

established as alternative substrate material for components in a wide range of technical applications like gears, sliding bearings or compressor plate valves under low tribological loads [1]. This is due to a high chemical and temperature resistance as well as promising mechanical properties for technical applications. However, this leads to high costs compared to other conventionally used polymers like polyamide 66 (PA66). This polymer possesses lower mechanical and chemical properties in relation to PEEK. Polyamide is often used for structural components and tanks in the automotive industry. Nevertheless, a disadvantage arises in the use of polymers in tribological systems due to the reduced load carrying capacity compared to metals. This is accompanied by increased wear of the polymers and thus limits the field of application under high loads.

There is a long-term effort to decrease wear of PEEK mainly by addition of various fillers, fibers and solid lubricants to form better performing composites [2–12]. The most often carbon and glass fibers are used for reinforcement and PTFE particles as a solid lubricant. Wear improvement up to three orders of magnitude and friction decrease by up to 75% were reported. Laux et al. showed that wear depends

✉ M. Thiex
publications@iot.rwth-aachen.de

S. Reitschuster
stefan.reitschuster@tum.de

¹ Surface Engineering Institute (IOT), RWTH Aachen University, Kackertstraße 15, 52072 Aachen, Germany

² Brno University of Technology (BUT), Technická 2896/2, 616 69 Brno, Czech Republic

³ Gear Research Center (FZG), Department of Mechanical Engineering, School of Engineering & Design, Technical University of Munich, Boltzmannstraße 15, 85748 Garching, Germany

on PEEK molecular weight and that sliding perpendicular to the roughness lay leads to thinner transfer film [13]. Zalaznik et al. pointed out that processing temperature influences hardness and tribological performance of PEEK [14].

A promising approach to increase the wear resistance of polymers is the application of physical vapor deposition (PVD) coatings, which enable a friction and wear reduction in tribological systems among others. Since the fields of application for polymers steadily increased during the 90 s, first analyses on PVD coating of thermoplastics like polycarbonate (PC), polybutylene terephthalate (PBT), polyamide (PA6.6) were conducted by Lugscheider et al. [15]. Therein the authors showed the possibility of depositing TiN on polymers by upscaling from a laboratory scale coating unit on an industrial unit. Riester et al. analyzed the influence of Ar, O₂ or N as plasma etching gases on the surface activation of PBT before coating and found the highest potential for surface activation using Ar or O₂ in contrast to N₂ [16]. Further analysis of Lugscheider et al. using a combined pulsed magnetron sputtering technology for the deposition of TiN on polymers like PA, PEEK amongst others showed an improved compound adhesion between coating and substrate material compared to the sole use of direct current (dc) or pulsed magnetron sputtering [17]. The deposition of a zirconium modified DLC coating on PEEK was analyzed for the targeted application on a PEEK based cage for spindle bearings [18]. Therein, the results demonstrate an improved adhesion between coating and PEEK after plasma etching with argon or alternatively an argon ethyne mixture combined with a radio frequency (RF) pulsed bias voltage. These basic research studies prove the possible application of PVD coatings on polymers by process parameter adjustments.

Also, first tribological analyses were conducted by Kapinski et al., testing a-C:H coated PA66 against uncoated 100Cr6 under dry conditions at an initial Hertzian pressure of $p_H = 160$ MPa [19]. The results prove that a-C:H coatings developed for steel substrates can be transferred to PA66 substrate and are able to reduce friction and wear and enhance lifetime. Kaczorowski et al. analyzed the effect of an O₂/CH₄ etching plasma compared to a N₂/CH₄ etching plasma on the surface activation and found, that remains of N₂ are integrated into the coating structure [20]. The addition of N₂ into the a-C:H coating also led to a friction reduction under dry conditions against zirconium oxide at a Hertzian pressure of $p_H = 117$ MPa compared to the use of an unmodified a-C:H coating. Another approach by Dufils et al. is texturing of a-C:H coated PEEK tested against alumina and lubricated with distilled water at a Hertzian pressure of $p_H = 53$ MPa [21]. It was found that dimples with a size between 12 and 21 μm and a density on the coated surface area between 10 and 30% lead to a significant friction reduction compared to uncoated PEEK. Tribological tests at higher initial Hertzian pressure of $p_H = 345$ MPa

under boundary and mixed lubrication against uncoated 100Cr6 also prove a friction and wear reduction compared to uncoated PEEK [22]. The overview of tribological investigations shows that DLC has a high potential to affect the wear and friction behavior of polymers positively. Nevertheless, there are only a few studies in this field so far, so that further investigations regarding the mechanical and chemical interactions during the tribological contact are necessary for a broad knowledge base.

Besides the achieved friction and wear reduction, the DLC microstructure is affected by the tribological contact conditions, which can be analyzed by means of Raman spectroscopy. The effect on the microstructure is called relaxation as described by Kalish et al. [23] and is dominated by the two main mechanisms clustering of graphitic sp² bindings and the transformation of diamond-like sp³ bindings into sp²-bindings. Furthermore, clustering subdivides itself into the three processes:

- Transformation of sp² chain bindings into sp² ring bindings
- Reduction of density and rearrangement of sp² bindings
- Effusion of hydrogen, which is only valid for hydrogen-containing DLC

The Raman spectrum of carbon is primarily determined by the presence of the G peak, which is based on bond stretching vibrations of chain and ring sp²-bindings [24]. The D peak is solely based on breathing modes of sp² ring bindings. Ferrari and Robertson analyzed the influences of different bonding states and composition of hydrogen-free amorphous carbon coatings [25]. Thereby, the position and intensity of D and G peak are affected by clustering, bond disorder, share of sp² chain bindings and sp³ bindings. A qualitative evaluation of the binding states of hydrogen-free DLC is possible through the 3-stage model established by Ferrari and Robertson. Therein, the G peak position and ratio of the intensities of G and D peak are considered to describe the amount of sp³ bindings in DLC. The interpretations of the 3-stage model are extended for hydrogen-containing DLC coatings by Casiraghi et al. [26]. Furthermore, the parameters dispersion of the G peak $\text{Disp}(G)$ and the full width half maximum $\text{FWHM}(G)$ of the G peak can be determined. The $\text{Disp}(G)$ predominantly describes the topological disorder, which combines the information of size and shape distribution of sp² clusters of chains. At the same time, changes of sp² ring bindings do not affect $\text{Disp}(G)$ based on the results for a hydrogenated DLC coating ta-C:H of Ferrari and Robertson [27]. Furthermore, also the structural disorder of amorphous carbon can be described by determining the full width half maximum of the G peak $\text{FWHM}(G)_{UV}$ under UV excitation. Based on the findings

of Casiraghi et al., structural disorder arises mainly from bond angle and bond length distortions [26]. It must be noted, that the influence of the structural disorder on the $\text{Disp}(G)$ and the topological disorder on the $\text{FWHM}(G)_{UV}$ cannot be completely excluded.

In this study, durable DLC coatings applicable on PEEK and PA66 substrates to improve tribological performance are developed. The a-C:H coated specimens were analyzed after tribological testing to identify possible changes in the coating structure and further correlated with findings based on frictional and wear behavior.

2 Methods

2.1 Pretreatment of PEEK and PA66 Specimens

Squared polymer samples of PEEK, TECAPEEK, Ensinger GmbH, Nufringen, Germany, and PA66, TECAMID 66 LA natural, Ensinger GmbH, Nufringen, Germany, with a size of $30 \text{ mm} \times 30 \text{ mm}$ and a height of $h = 8 \text{ mm}$ were grinded and polished by means of Phoenix 4.000 \times , ITW Test & Measurement GmbH, Esslingen am Neckar, Germany, to a roughness of $R_a \approx 0.05 \mu\text{m}$. Therefore, SiC paper with a grain size of 1200, 2000 and 4000 and diamond suspension with a grain size of $3 \mu\text{m}$ was used. The samples were chemically purified in a cleaning unit with the water-soluble basic detergents GALVAPREP SU 2012, NGL Cleaning Technology SA, Nyon, Switzerland, and a subsequent washing with water and isopropanol $\text{C}_3\text{H}_8\text{O}$.

2.2 Coating Process

Two a-C:H coatings, called a-C:H-1 and a-C:H-2, were developed and deposited in an industrial scale coating unit CC800/9 Custom, CemeCon AG, Wuerselen, Germany. The coating unit was equipped with two high power pulsed magnetron sputtering (HPPMS) cathodes. The arrangement of the cathodes and the layout of the deposition chamber are depicted in Fig. 1. For the deposition of the a-C:H coatings, four C targets with a purity of $\text{C} = 99.9\%$ were used. The process and reactive gases were argon (Ar), helium (He) and ethyne (C_2H_2). The coating processes were adjusted in accordance with mechanical properties, which show higher values for PEEK in comparison to PA66. A reduced helium gas flow lowers the degree of ionization of carbon in the coating process. The resulting structure shows a reduced content of diamond-like sp^3 bindings in favor of more graphitic sp^2 bindings. The reduction of the bias voltage U_B influences the morphology as well as the mechanical properties due to the lower kinetic energy of the ionized particles during the coating growth.

The helium gas flow was reduced from $Q = 70 \text{ sccm}$ to $Q = 50 \text{ sccm}$ and the bias voltage from $U_B = -250 \text{ V}$ to $U_B = -200 \text{ V}$ for the deposition on PA66, Table 1. In addition, the bias voltage U_B was pulse-synchronized with the HPPMS cathodes, which reduces the thermal transfer on the substrate material. The PVD coating process is basically divided into the four steps heating, etching, coating and cooling. In between the steps heating and etching there is a process step called off-gassing, where the starting pressure of $p = 3 \text{ mPa}$ is reached again. In order to analyze the substrate temperature monitored during the coating

Fig. 1 Schematic representation of the industrial coating unit CC800/9 Custom and target

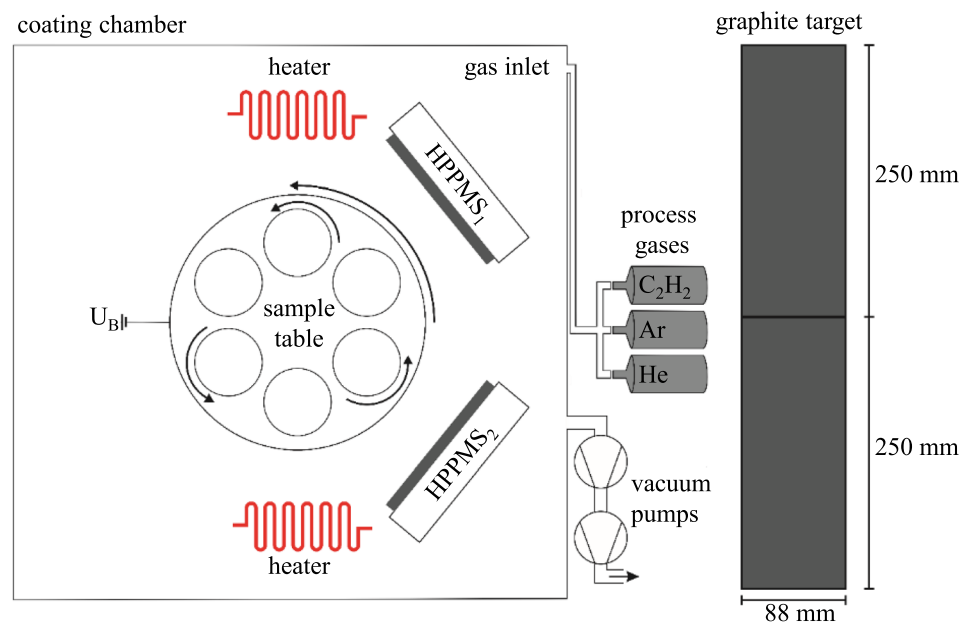


Table 1 Process parameters of a-C:H-1 on PEEK and a-C:H-2 on PA66 shown in [22]

Process parameter and unit	a-C:H-1 on PEEK	a-C:H-2 on PA66
Argon gas flow, Q_{Ar} in sccm	200	200
Process pressure, p in mPa	500	500
Ethyne gas flow, $Q_{C_2H_2}$ in sccm	10	10
Helium gas flow, Q_{He} in sccm	70	50
HPPMS cathode power, P in W	4000	4000
Pulse-on-time, t_{on} in μ s	100	100
Frequency, f in Hz	500	500
Bias voltage, U_B in V	- 250	- 200
Coating time, t in s	7200	7200

process, temperature measurements were carried out using Insitemp, which is described in [28]. Therefore, specimen dummies made out of PEEK and PA66 were used.

2.3 Coating Analysis

The coating thicknesses and morphology were analyzed by scanning electron microscopy (SEM), Oxford Link ISIS, Oxford Instruments plc, UK, at the Central Facility for Electron Microscopy (GfE), RWTH Aachen University, Aachen, Germany. A nanoindenter of type TI 950 TriboIndenter, Bruker Corporation, Billerica, Massachusetts, USA, with a Berkovich indenter with a nominal edge radius of approximately $R = 20$ nm was applied for the determination of the indentation hardness H_{IT} and modulus of indentation E_{IT} . The samples were unprepared and the used constant indentation force was $F = 2$ mN. Thereby, the penetration depth was kept below 10% of the top layer thickness. Thus, the influence of the substrate material can be minimized as explained by Fischer-Cripps [29]. In order to determine H_{IT} and E_{IT} , $x = 40$ individual measurements were conducted and subsequently averages out of the force–displacement curves were calculated. Calculations of the modulus of indentation are based on Oliver and Pharr's equations [30]. Further informations on the nanoindentation method are presented in [31]. A constant Poisson's ratio of $\nu = 0.25$ was assumed for the coatings. Nuclear reaction analysis (NRA) were carried out at Helmholtz Zentrum Dresden Rossendorf (HZDR), Dresden Rossendorf, Germany, to determine the hydrogen content of the a-C:H coatings in the as-deposited status. Two positions were analyzed on each coating for the penetration depths $\gamma = 35$ nm and $\gamma = 500$ nm with 20 repetitions. Thereby, the resulting hydrogen contents had to be evaluated by an exponential fitting method with approximation

Table 2 Properties of the considered mineral oil FVA3 [32]

Characteristic value and unit	FVA3
Kinematic viscosity ν (40 °C) in $\text{mm}^2 \text{s}^{-1}$	95
Kinematic viscosity ν (60 °C) in $\text{mm}^2 \text{s}^{-1}$	40
Kinematic viscosity ν (100 °C) in $\text{mm}^2 \text{s}^{-1}$	11
Density ρ in g cm^{-3}	0.90 ($\vartheta_{Oil} = 15$ °C)

to a limit value in contrast to the determination by mean value.

2.4 Compound Analysis

The analysis of the compound adhesion between the a-C:H coatings and PEEK respectively PA66 were conducted by means of scratch tester Gesellschaft für Fertigungstechnik und Entwicklung Schmalkalden e.V. (GFE), Schmalkalden, Germany. Scratch tests, with one repetition each, were conducted with a Rockwell C diamond at different constant forces between $10 \leq F_N \leq 250$ N in steps of 10 N. Every scratch was generated with a length of $x_s = 4$ mm and a feed speed $v_f = 10$ mm min^{-1} . The load was applied during the first $x_s = 0.2$ mm of the total scratch length. In accordance to DIN EN ISO 20502, the compound adhesion between coating and substrate was evaluated by scratch tests and confocal laser scanning microscopy (CLSM), VK-X210, Keyence, Neu-Isenburg, Germany. It has to be stated that the scratch testing is not standardized for coated plastics. Nevertheless, the indentation and scratching with a Rockwell C diamond through coated plastics at different loads simulates a high stress collective for the compound of coating and substrate material.

2.5 Tribological Analysis by Means of Pin-on-Plate Tribometer

Reciprocating pin-on-plate (PoP) tribological tests were carried out on an UMT Tribolab, Bruker Nano, California, San Jose, USA, under dry and lubricated conditions. In the device, normal load is close-loop controlled and measured simultaneously with friction by two axis sensor. The pin is stationary and the plate performs a harmonic motion. A circular point contact was formed between 10 mm in diameter 100Cr6 bearing steel ball and flat coated and uncoated PEEK and PA66 specimens with a geometry 30×30 mm and height of $h = 8$ mm. Dry and oil lubricated conditions were measured. A mineral base oil FVA3 was used as lubricant, Table 2. Operating conditions of the tests are listed in Table 3. Tribological performance over time was studied in five steps of test duration.

Table 3 Operating conditions of PoP tribological tests

Characteristic value and unit	Dry	Lubricated
Lubricant	–	FVA3
Test temperature T in °C	60	90
Relative humidity RH in %	40	-
Frequency f in Hz	2	2
Stroke δ in mm	2.2	2.2
Mean speed v in m s ⁻¹	0.01	0.01
Load F in N	25	25
Test duration $N \triangleq$ number of passes	{1,600; 3,200; 8,000; 16,000; 32,000}	

In initial tests, a higher frequency compared to $f=2$ Hz was tested. It led to wear tracks that have signs of wear markedly influenced by contact temperature rise, thus the frequency was decreased to $f=2$ Hz. The test temperature for oil lubricated conditions was set to $\vartheta_{\text{Oil}}=90$ °C to decrease oil viscosity and minimize formation of fluid film. The goal was to perform tests at severe mixed and boundary lubrication (see Table 3).

The average coefficient of friction and volume of material removed by wear were evaluated. The wear volume was evaluated from surface topography measurement of the complete wear track after the experiment by optical profilometer Contour GT-X8, Bruker, Arizona, Tucson, USA. To be precise, the wear volume was evaluated as a net missing volume of material from topography data with reference plane established on surface out of the wear track. In this way of evaluation, the transported material on the plate is not included in the wear volume. The volume was calculated from the area of wear track and the closest surroundings by masking out the rest of sample. This approach decreases uncertainties of the volume measurement due to surface geometry imperfections (waviness). The estimated uncertainty of wear volume is around $1 \cdot 10^5 \mu\text{m}^3$. It is mainly given by precision of reference plane establishment and local sample waviness in the area of wear testing.

2.6 Chemical Analysis After Tribological Testing by Means of Raman Spectroscopy

The molecule structure of the hydrogen-containing amorphous carbon coatings before and after tribological testing was analyzed by means of Raman spectroscopy. Therefore, the Raman spectrometer, Renishaw InVia Reflex, Renishaw GmbH, Plietzhausen, Germany, with a $\lambda_{\text{VIS}}=532$ nm laser with a spot size of $d \approx 1 \mu\text{m}$ and a diffraction grating $g_{\text{VIS}}=1800 \text{ l mm}^{-1}$ was used. In addition, Raman spectra were taken with an ultraviolet (UV) laser $\lambda=325$ nm with a spot size $d \approx 6 \mu\text{m}$ and a diffraction grating $g_{\text{UV}}=2400 \text{ l mm}^{-1}$. The lasers were calibrated before the measurement using a silicon reference

sample. To enable an evaluation of statistic valid data, a mapping measuring method was used. Hereby, a matrix with 2×3 measurement points with size of $100 \times 100 \mu\text{m}$ and a step width of $50 \mu\text{m}$ was positioned horizontal over the middle of the wear track on a-C:H coated disk for the analysis by VIS and UV laser. The measurement parameters are shown in Table 4.

For visible light (VIS) laser excitation the G peak position ranges between $1560 \text{ cm}^{-1} \leq \tilde{\nu}_{\text{G,VIS}} \leq 1600 \text{ cm}^{-1}$ and in the area between $1600 \text{ cm}^{-1} \leq \tilde{\nu}_{\text{G,UV}} \leq 1690 \text{ cm}^{-1}$ using an ultraviolet (UV) laser. The D peak occurs in the area $1360 \text{ cm}^{-1} \leq \tilde{\nu}_{\text{D}} \leq 1400 \text{ cm}^{-1}$ under VIS excitation, as far as ring bindings are present in the DLC structure. Higher wave numbers of the D peak position are measured by UV laser excitation in the area between $1400 \text{ cm}^{-1} \leq \tilde{\nu}_{\text{D,UV}} \leq 1500 \text{ cm}^{-1}$.

All spectra were taken using the software Wire® 5.4, Renishaw plc, Wotton-under-Edge, United Kingdom. Thereby, the spectra were evaluated section by section of the Raman shift by a combined Gaussian and Lorentzian fitting. Based on the measured spectra, the parameters $I(\text{D})/I(\text{G})_{\text{VIS}}$ ratio, $I(\text{D})/I(\text{G})_{\text{UV}}$ ratio, $\text{FWHM}(\text{G})_{\text{UV}}$ and $\text{Disp}(\text{G})$ were determined. In case of the characteristic value $\text{FWHM}(\text{G})_{\text{UV}}$, the UV excitation enables to exclude the photoluminescence of the spectra as shown by Casiraghi et al. [26]. Furthermore, the dispersion of the G peak $\text{Disp}(\text{G})$ can be calculated by determining the position at visible light $\tilde{\nu}_{\text{G}}$ and UV $\tilde{\nu}_{\text{G,UV}}$ excitation divided by the excitation wavelengths.

The interpretations of the a-C:H coatings were performed in analogy to the findings of Casiraghi et al. [26]. Correspondingly, the coatings were classified as graphite-like a-C:H (GLCH) with a hydrogen content $\Psi > 20\%$ and sp^2 clustered ring bindings.

$$\text{Disp}(\text{G}) = \frac{\tilde{\nu}_{\text{G,UV}} - \tilde{\nu}_{\text{G}}}{\lambda_{\text{UV}} - \lambda} \left[\frac{\text{cm}^{-1}}{\text{nm}} \right] \quad (\text{G1. 1})$$

Table 4 Raman measurement parameters for chemical analysis of a-C:H coatings before and after tribological testing

Characteristic value and unit	Vis	UV
Wavelength λ in nm	532	325
Laser power P_{L} in mW	2.6	3
Accumulations N	1	3
Exposure time t_{E} in s	10	10

3 Results and Discussion

3.1 Coating and Compound Analysis

3.1.1 Substrate Temperature Measurement During Coating Process

The results of the substrate temperature measurement during the coating processes of PEEK and PA66 are shown in Fig. 2. Thereby, the coating process is divided into the five phases heating, off-gasing, etching, coating and cooling. The highest substrate temperature for a-C:H-1 is reached during the etching phase with $T_{\max,1} = 174\text{ }^{\circ}\text{C}$, whereby the maximum substrate temperature for a-C:H-2 was measured at $T_{\max,2} = 186\text{ }^{\circ}\text{C}$. It is believed, that the deviation between the maximum substrate temperatures results predominantly from differences of the PEEK and PA66 specimen properties and to a minor extend due to differences in the coating processes.

In general, the measured substrate temperatures are far below the melting temperatures of PEEK with $T = 340\text{ }^{\circ}\text{C}$ and PA66 with $T = 255\text{ }^{\circ}\text{C}$, given by Domininghaus et al. [1]. In contrast thereto, the glass transition temperatures of PEEK with $T = 143\text{ }^{\circ}\text{C}$ and PA66 with $T = 70\text{ }^{\circ}\text{C}$ are surpassed. On this point, it must be stated that the PEEK and PA66 specimens are mounted using holders which allow movement such that no significant thermal stresses occur during coating process.

3.1.2 Morphology of a-C:H Coatings by SEM Analysis

The cross-sectional images and top layer images of a-C:H-1 and a-C:H-2 are shown in Fig. 3. Thereby a columnar structure with the transition into an amorphous character of both coatings a-C:H-1 and a-C:H-2 can be observed.

The cross-sectional image for a-C:H-1 shows a wavy structure and it can be assumed that this is caused by the

preparation of the specimens for the microscopy. Hereby, it is necessary to apply high mechanical forces to break the specimens. Even though there are high plastic deformations of the substrate material visible, no cracking or delamination at the interface between coating and substrate can be observed. At the top view of a-C:H-1 interspaces can be seen in between the cauliflower structure, which can be a result of the sample preparation during grinding and polishing. A coarse columnar structure can be observed for a-C:H-2 on PA66. Furthermore, a very rough structure can be seen at the top layer of a-C:H-2, where the columns show locally heightened areas. It can be assumed, that among others the structural differences between a-C:H-1 and a-C:H-2 result from the growth process on the ring binding structure of PEEK and chain binding structure of PA66. The coatings should be predominantly composed of sp^2 ring bindings due to the HPPMS sputtering of graphite in contrast to the share of sp^2 chain bindings resulting out of the low ethyne gas flow with $\dot{Q}_{\text{C}_2\text{H}_2} = 10\text{ sccm}$. Thus, the “epitaxial” coating growth of a-C:H-2 on PA66 is affected in comparison to the coating growth of a-C:H-1 on PEEK and leads to the observed uneven structure. Due to the small differences of bias voltage with $\Delta U_{\text{B}} = 50\text{ V}$ and helium gas flow with $\Delta \dot{Q}_{\text{He}} = 20\text{ sccm}$ compared to a-C:H-1, it is not believed, that the process parameters lead to the observed changes of the coating structure. Catena et al. came to a similar conclusion by analyzing the structure of a-C:H on different thermoplastic substrate materials like polyoxymethylene (POM), high density polyethylene (HDPE) and polyethylene terephthalate (PET) [33].

3.1.3 Roughness of Uncoated and Coated Samples

The results of the roughness measurements of the arithmetical mean roughness R_a and root mean square roughness R_q

Fig. 2 Substrate temperature during coating process of a-C:H-1 and a-C:H-2

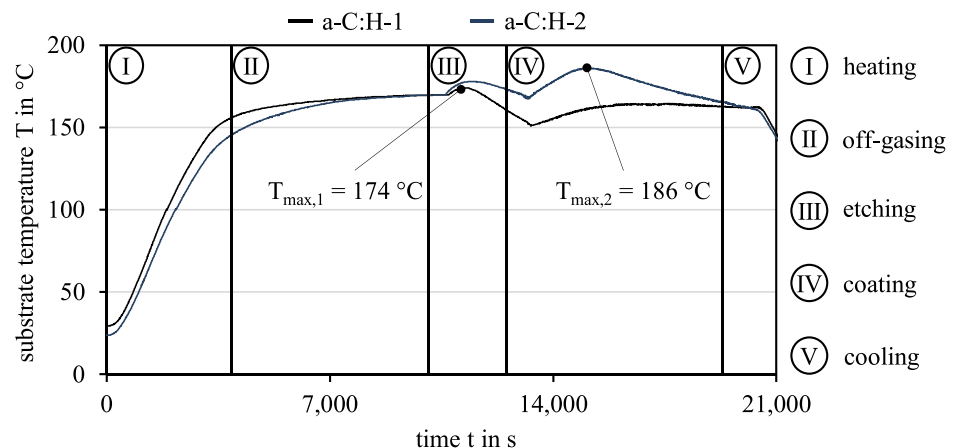


Fig. 3 Cross sectional images and topography images of a-C:H-1 on PEEK, shown in [22], and a-C:H-2 on PA66

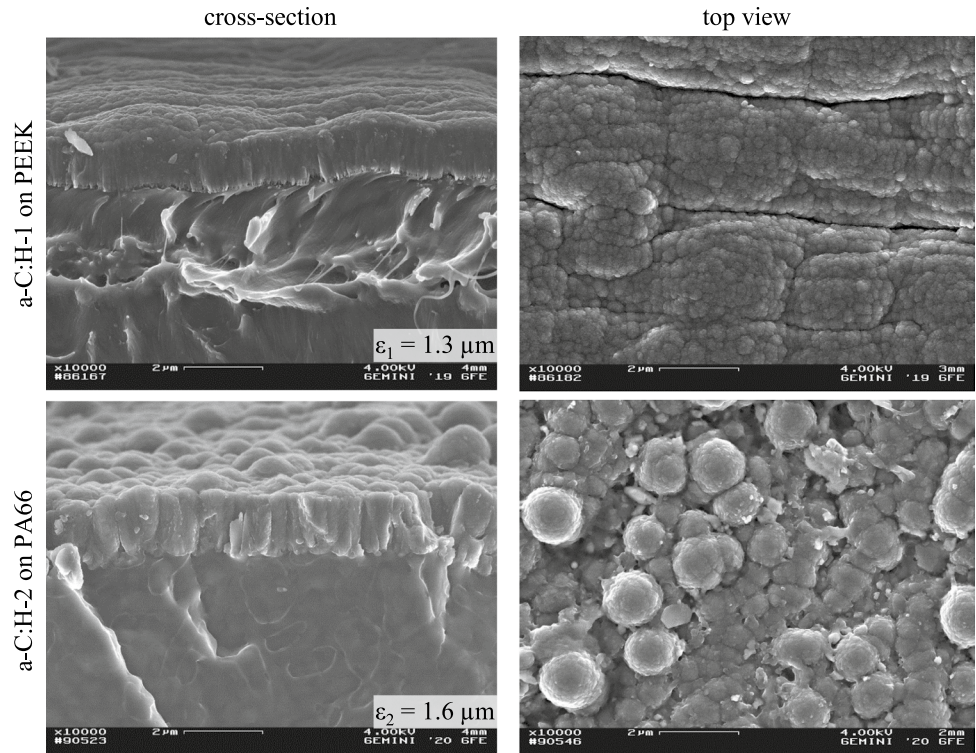
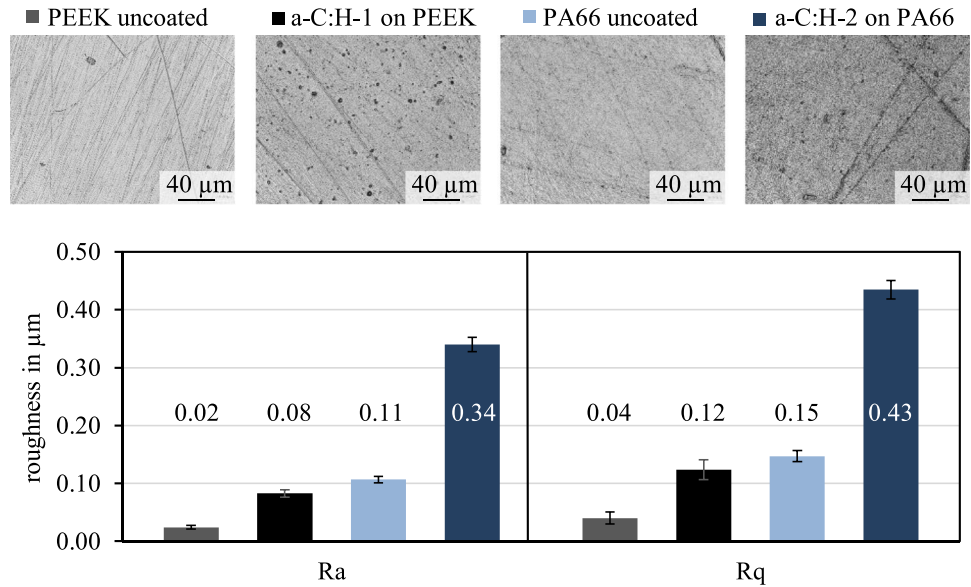


Fig. 4 Roughness measurement of uncoated and coated PEEK and PA66



before and after coating of PEEK and PA66 are shown in Fig. 4. The increase in roughness for the as-deposited state of a-C:H-1 compared to uncoated PEEK is moderate.

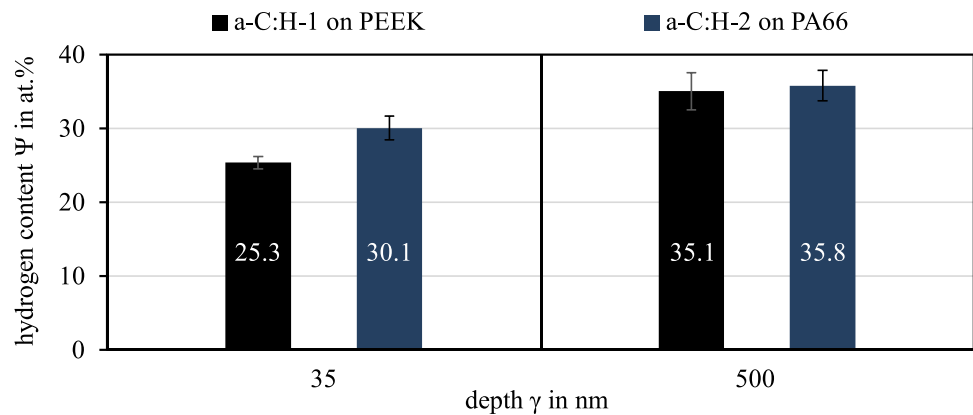
An explanation can be given by small defects on the a-C:H-1 coating, which result out of the coating growth process. In contrast, the roughness of the PA66 specimen increases significantly after coating deposition. The measurements of Rq show a similar trend to the changes of Ra.

Overall, the roughness measurements confirm quantitatively the observations of the SEM images.

3.1.4 Chemical Analysis of Hydrogen Content of a-C:H Coatings

The hydrogen content Ψ of a-C:H-1 and a-C:H-2 at $\gamma = 35$ nm and $\gamma = 500$ nm depths from the top layer are

Fig. 5 Hydrogen content of a-C:H-1 and a-C:H-2 at different depths



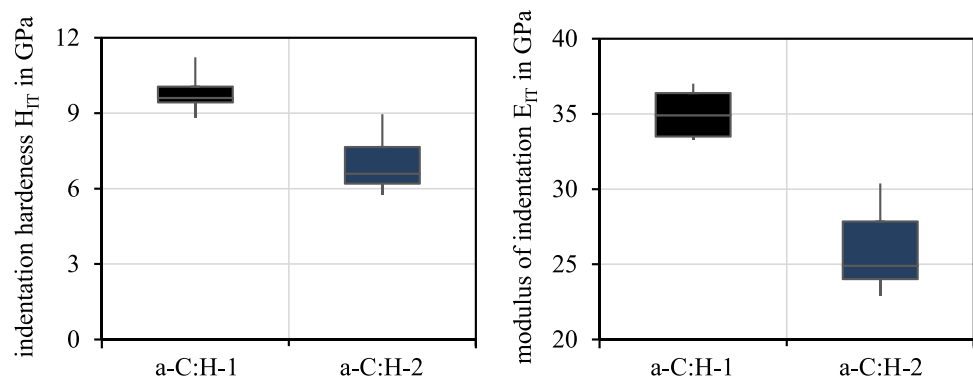
shown in Fig. 5. It can be observed, that the hydrogen content at the top layer in $\gamma=35$ nm depth varies between $\Psi \approx 5.0$ at.% by comparing a-C:H-1 and a-C:H-2. By increasing the penetration depth to $\gamma=500$ nm the hydrogen contents of both coatings tend to equalize. It can be assumed, that the deviations of the hydrogen content at the top layer result from the differences of the coating process parameters as well as the substrate material properties of PEEK and PA66 on the coating growth process.

Information about the binding structure of hydrogen in the a-C:H coatings could be obtained out of the evaluation of the hydrogen content. Based on extrapolation method against zero, the absolute hydrogen contents could be calculated. The reason for the exponential fitting method is due to an effusion of hydrogen during the measurement, which indicates that hydrogen is primarily interstitial embedded in the a-C:H coating structure. It can be assumed, that this enables an easier effusion to the surface and affects the tribological behavior.

3.1.5 Indentation Hardness and Modulus of Indentation of a-C:H Coatings

The indentation hardness H_{IT} and the modulus of indentation E_{IT} of the DLC coatings are shown in Fig. 6. In order to

Fig. 6 Indentation hardness H_{IT} and modulus of indentation E_{IT} of a-C:H-1 on PEEK and a-C:H-2 on PA66 shown in [22]

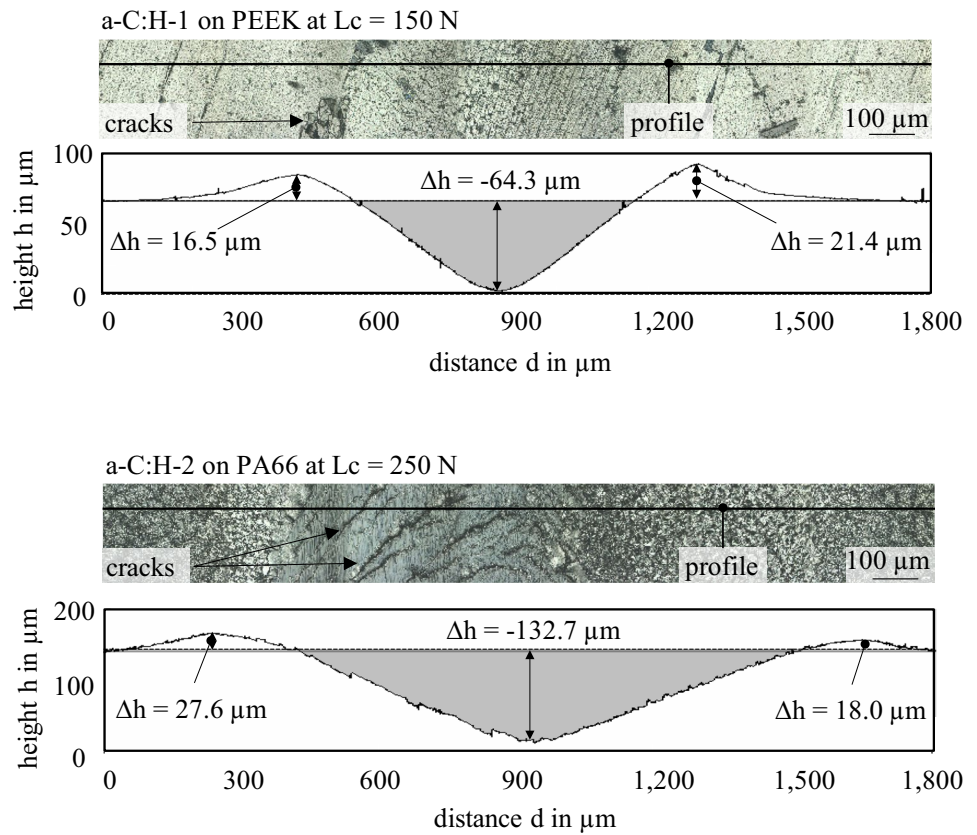


minimize an influence of the substrate material on the hardness measurement, the penetration depth of the Berkovich indenter was kept at 10% of the individual coating thickness. The difference between the indentation hardness and the modulus of indentation of a-C:H-2 compared to a-C:H-1 can be explained based on the reduced helium gas flow and changed bias voltage U_B during the coating process. The changes lead to a lower ionization energy of the C-C and C-H clusters in the a-C:H-2 coating process, which negatively affects the formation of sp^3 diamond bindings and reduces the share in relation to the sp^2 bindings. In addition, the hydrogen content at the top layer is higher for a-C:H-2 in contrast to a-C:H-1, which also reduces the hardness of the coating.

3.1.6 Compound Adhesion of a-C:H on Polymers

The compound adhesion between a-C:H-1 and PEEK as well as a-C:H-2 and PA66 was tested by means of scratch testing, Fig. 7. Even though the scratch test is not standardized for the analysis of coated polymers, important insights can be gained. The results show a high deformation of $\Delta h = -64.3$ μm of the a-C:H-1 on PEEK compound at a critical load $L_c = 150$ N in the center of the scratch without a coating delamination. In the edge regions of the scratch,

Fig. 7 Compound adhesion between a-C:H-1 on PEEK and a-C:H-2 on PA66



high plastic deformation up to a height of $h=21.4 \mu\text{m}$ only show partial cracks of a-C:H-1.

With regard to the a-C:H-2 on PA66 compound, higher critical loads up to $L_c=250 \text{ N}$ could be applied without coating delamination. Higher critical loads also result in increased plastic deformation up to $\Delta h=-132.7 \mu\text{m}$. At $L_c=250 \text{ N}$, the maximum load of the analyzing unit was achieved. Nevertheless, the elevations at the edge of the scratch remain at a comparable level around $\Delta h \approx 20 \mu\text{m}$ compared to the a-C:H-1 on PEEK compound. In the case of a-C:H-2 on PA66 compound, cracks form at the top layer within the left side of the scratch and not in the edge region.

Both a-C:H coatings are able to undergo high deformation without delaminating from the polymers and significant differences in the hardness and modulus of indentation. This offers a high potential for a subsequent tribological analysis under high loads, to investigate the effect on friction and wear in highly stressed sliding and rolling-sliding contacts.

Fig. 8 a Wear volume and b coefficient of friction of PEEK/100Cr6 and a-C:H-1/100Cr6 under dry conditions

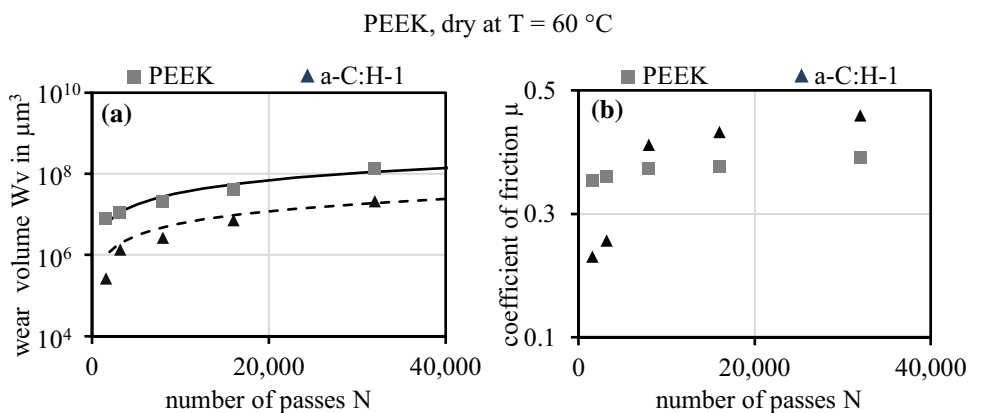
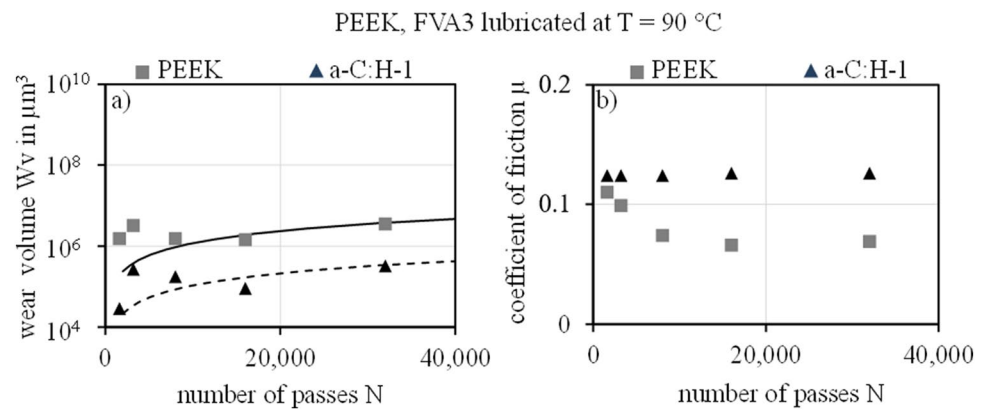


Fig. 9 **a** Wear volume and **b** coefficient of friction of PEEK/100Cr6 and a-C:H-1/100Cr6 under lubricated conditions



3.2 Tribological Behavior and Evaluation

3.2.1 Friction and Wear Measurements

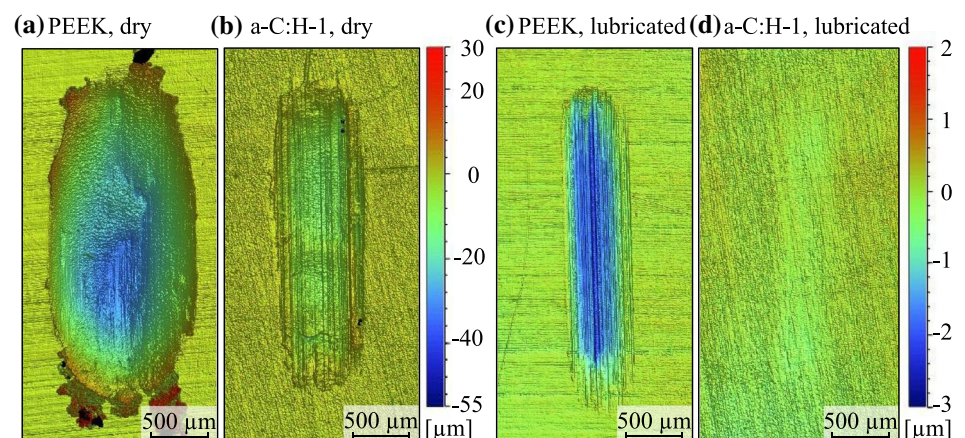
The results of wear volume and the average coefficient of friction μ depending on the number of passes for uncoated PEEK and a-C:H-1 on PEEK under dry conditions at $T = 60\text{ }^{\circ}\text{C}$ are shown in Fig. 8. Solid and dashed lines show the linear fits with the wear rates to the data of PEEK and a-C:H-1 respectively, whereby the y axis is in log scale.

Wear is approximately one order of magnitude lower for coated than for uncoated PEEK for all measured passes. The coefficient of friction is at an almost constant level for PEEK/100Cr6, whereas an increase with the number of passes for a-C:H-1/100Cr6 can be observed. As the number of passes N exceeds 8000, the coefficient of friction of a-C:H-1/100Cr6 is lightly increased compared to PEEK/100Cr6. Due to high hardness of a-C:H-1 coating and 100Cr6 ball, both surfaces undergo transformations during wear process under dry lubrication. Therefore, a possible explanation for increase of friction can be an increase of abrasive wear. The latter would be connected with change in tribofilm chemistry. No dedicated analyses were made to chemistry of tribofilms in this study. Figure 9 shows the wear

volume and coefficient of friction for lubricated conditions at $T = 90\text{ }^{\circ}\text{C}$. The pairing of a-C:H-1/100Cr6 features lower wear by approximately one order of magnitude compared to PEEK/100Cr6. When compared to dry conditions, the wear volumes are about one and a half orders of magnitude lower. The coefficient of friction is stable for a-C:H-1/100Cr6 and there can be seen a slight increase and leveling off for PEEK/100Cr6. In this pairing, the wear occurs primarily at the PEEK specimen. A significant wear track with scratch topography (Fig. 10c) is produced for high number of passes. The decrease of friction can be connected with improved lubrication due to PEEK surface adaptation to the steel pin, and thus, operation of the contact with less solid contacts.

Fig. 10 shows surface height images of uncoated and coated PEEK after wear testing for $N = 16,000$. The reason for the selection of $N = 16,000$ passes is that this is a representative mid-point of the analyses, as Figs. 8 and 9 show that an increase in the number of passes lead to comparable or minimally increased values. The wear track on uncoated PEEK shows high plastic deformation and a transport of material towards the edge regions under dry conditions. The average rise in contact temperature due to friction is higher under dry conditions compared to lubricated conditions. The uncoated PEEK sample has

Fig. 10 Wear tracks on uncoated PEEK and a-C:H-1 after $N = 16,000$ passes; **a** and **b** for dry conditions; **c** and **d** for lubricated conditions



the highest wear scar depth in the center while the coated sample a-C:H-1 shows no major signs of deformations. Visible abrasion marks can be found on a-C:H-1 after dry testing and uncoated PEEK after lubricated testing. The a-C:H-1 coating decreases wear significantly under both lubrication methods.

The results of wear volume and the average coefficient of friction depending on the number of passes for PA66/100Cr6 and a-C:H-2/100Cr6 under dry conditions at $T = 60\text{ }^{\circ}\text{C}$ are shown in Fig. 11. Plotted solid and dashed lines are best fit linear trend lines of the wear data. Both samples follow an almost linear wear trend, note that y axis is in log scale. The wear volume for a-C:H-2 coated sample is significantly lower than for uncoated counterpart. The uncoated and coated configurations have a similar progressive trend of the coefficient of friction over the number of passes, whereas friction for a-C:H-2/100Cr6 is slightly lower compared to PA66/100Cr6.

The wear and friction performance is different under lubricated conditions, see Fig. 12. The wear volume of uncoated PA66 and a-C:H-2 is almost identical. However, the coefficient of friction of a-C:H-2/100Cr6 is higher but stable compared to PA66/100Cr6. The trend of increasing friction for a-C:H-2/100Cr6 with increasing number

of passes is similar to a-C:H-1/100Cr6, see Fig. 9. Thus, similar explanation can be expected.

The surface height images of wear tracks after $N = 16,000$ passes are shown in Fig. 13. For dry conditions, both wear tracks show elevated edge regions formed by wear debris. Some cracking and partial coating removal was visible for a-C:H-2/100Cr6 operating under dry conditions. It seems that surface defects and grooves support initiation of cracking but it is not possible to exclude also initiation on a regular surface. Since the cracking was not observed for a-C:H-1 coated PEEK and a-C:H-2 coated PA66 under lubricated conditions it is assumed that the cracking and partial coating removal is related to thermal properties of PA66. Abrasion scratch marks are visible dominantly for uncoated PA66 under lubricated conditions.

The DLC coating a-C:H-1 under dry conditions was exemplarily chosen for further analysis, due to the significant wear reduction compared to uncoated PEEK. Therefore, SEM and Raman analysis of the a-C:H-1 coating after $N = 16,000$ passes were conducted.

3.2.2 SEM and Raman Analysis of a-C:H-1

SEM topography and cross-sectional images of a-C:H-1 on PEEK after $N = 16,000$ passes are shown in Fig. 14. Several

Fig. 11 a Wear volume and b coefficient of friction of PA66/100Cr6 and a-C:H-2/100Cr6 under dry conditions

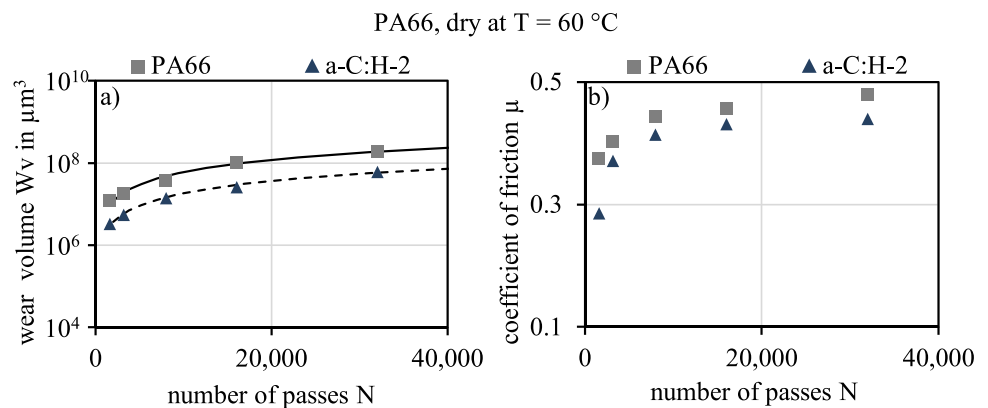


Fig. 12 a Wear volume and b coefficient of friction of PA66/100Cr6 and a-C:H-2/100Cr6 under lubricated conditions

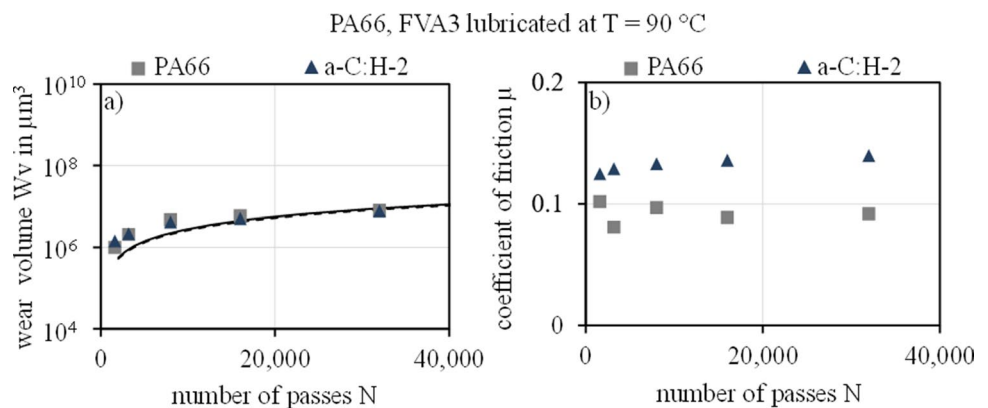


Fig. 13 Wear tracks on uncoated PA66 and a-C:H-2 after $N=16,000$ passes; **a** and **b** for dry conditions; **c** and **d** for lubricated conditions

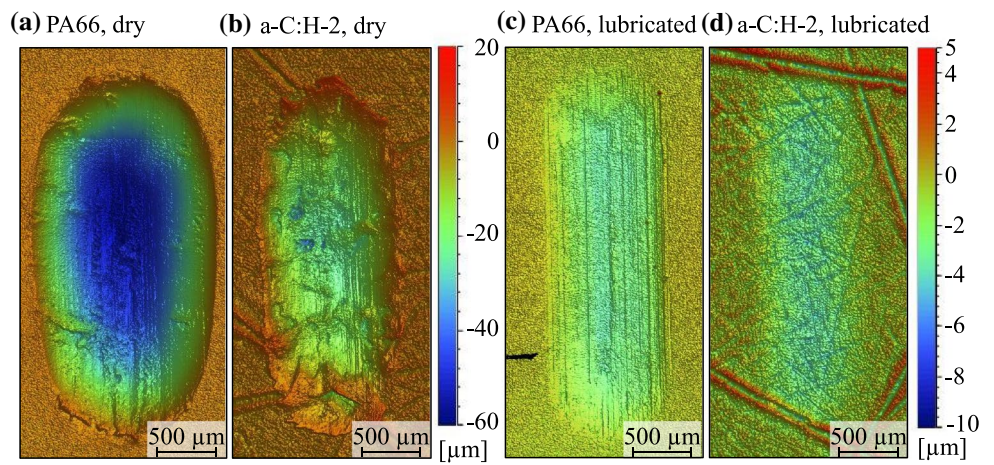
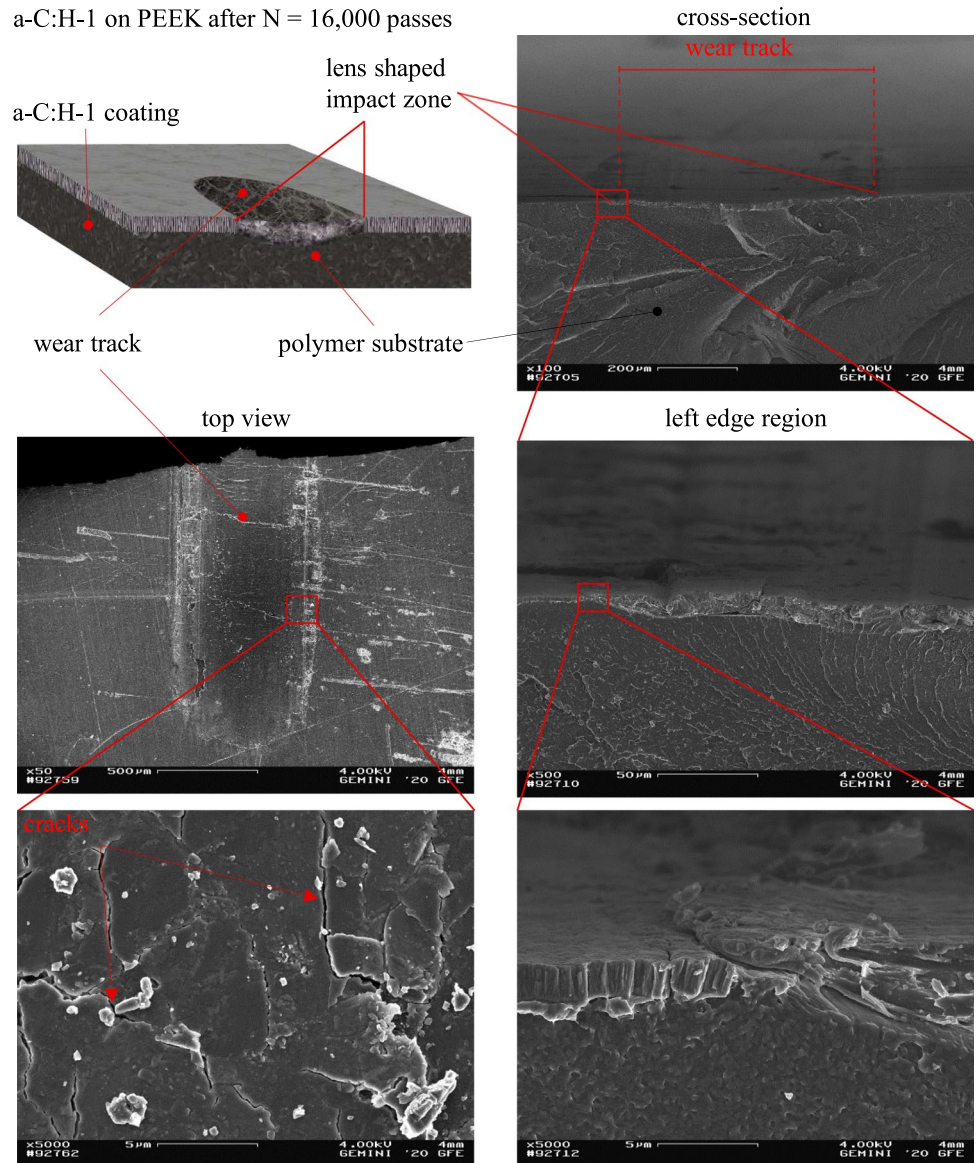


Fig. 14 Topography and cross section of wear track on a-C:H-1 on PEEK under dry conditions after $N=16,000$ passes



cracks can be identified inside the wear track on the topography images. Here, smaller detachments of the coating from the substrate material can also be seen in individual cases. The single columns of the cauliflower structure and the PEEK seem to have formed a composite layer. Changes in the mechanical properties could result from this, which favor the formation of cracks. This requires further investigation to gain a deeper understanding of the tribological behavior of the DLC coated thermoplastics.

With regard to the cross-sectional micrographs, this hypothesis can be confirmed: A lens shaped zone of impact with an amorphous structure can be identified within the wear track. Here, the interface between a-C:H-1 and PEEK can not longer be clearly differentiated from each other. The transition from the unloaded zone to the wear track can be observed in the left edge region. Raman measurements inside the wear track on a-C:H-1 prove, that the position and shape of the G peak changes significantly, Fig. 15. Evaluated data from the Raman spectra of a-C:H-1 as-deposited and a-C:H-1 after $N=16,000$ passes are shown in Table 5. In general, the spectrum after $N=16,000$ passes differs significantly from the uncoated PEEK spectrum and is more related to the a-C:H-1 as-deposited spectrum.

The G peak shifts about $\Delta\tilde{\nu}_G = 115 \text{ cm}^{-1}$ from the as-deposited state to the status after $N=16,000$ passes, which can be assigned to an increased clustering of the C–C and C–H bindings in the a-C:H-1 composite layer. The reason for this is the high Hertzian pressure and high frictional heat during dry contact conditions, which was calculated up to $T=152 \text{ }^\circ\text{C}$ based on the average temperature rise in accordance with [34]. Thus, the sp^2 chain bindings are transformed into sp^2 ring bindings, whereby the effusion of hydrogen additionally occurs. Furthermore, metastable sp^3 bindings transform into sp^2 ring bindings. The increasing share of sp^2 ring bindings can be additionally confirmed by the growing pronunciation of the D peak, which is solely based on vibrations of sp^2 ring bindings. However, the effect of increasing D peak can not be observed in the $I(\text{D})/I(\text{G})$ ratios whether under visible light or UV excitation. With regard to

Table 5 Results of Raman spectra evaluation

Characteristic value and unit	a-C:H-1 as-deposited	a-C:H-1 after $N=16,000$ passes
$I(\text{D})/I(\text{G})_{\text{VIS}}$ ratio	0.75 ± 0.01	0.66 ± 0.01
$I(\text{D})/I(\text{G})_{\text{UV}}$ ratio	0.55 ± 0.04	0.49 ± 0.05
$\text{FWHM}(\text{G})_{\text{UV}}$ in cm^{-1}	219.82 ± 5.65	208.63 ± 1.88
$\text{Disp}(\text{G})$ in $\text{cm}^{-1} \text{ nm}^{-1}$	0.48 ± 0.02	0.68 ± 0.02

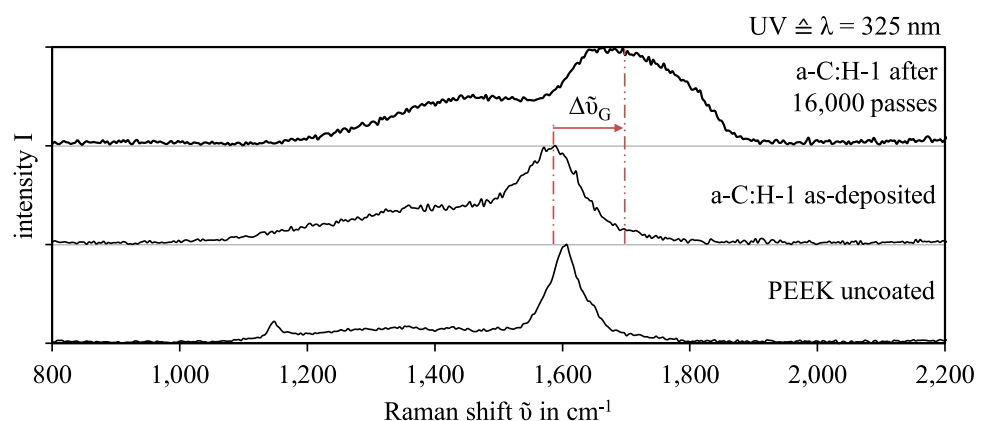
the shown Raman spectra, an increase of the FWHM would have been expected. However, the FWHM reduces from the as-deposited state compared to the after $N=16,000$ passes.

The increase of the $\text{Disp}(\text{G})$ is a result of the increased share of sp^2 ring bindings, whereby the size and shape distribution of the sp^2 clusters is changed as a consequence of the tribological load. An explanation for the unexpected observations of the $I(\text{D})/I(\text{G})$ ratios and the $\text{FWHM}(\text{G})_{\text{UV}}$ could be a mutual neutralization of the described effects. A further explanation, leading to possible misinterpretations of the considered Raman values could be the formation of the composite layer between a-C:H-1 and PEEK in the wear track due to high energy input. However, the application of a-C:H-1 still enables wear protection of PEEK. So far, these changes cannot be interpreted in terms of a positive or negative influence on tribological behavior, thus further studies are required.

4 Conclusions

In this study two a-C:H coatings were developed and tailored to the application on PEEK and PA66. Tribological analyses under dry and boundary lubricated conditions were conducted with focus on the friction and wear behavior. Finally, SEM and Raman analysis enabled a deeper

Fig. 15 Raman spectra of uncoated PEEK and a-C:H-1 on PEEK in different states



understanding of the effects of dry contact conditions on the a–C:H coatings. The results show:

- High plastic deformation of a–C:H coatings without delamination from the thermoplastic substrates PEEK and PA66
- Significant wear reduction under highly stressed dry and boundary lubricated conditions due to the application of tailored a–C:H coatings
- Possible formation of a composite layer of a–C:H-1 and PEEK in the wear track due to high energy input under dry conditions
- Transformation from sp^2 chain into sp^2 ring bindings as well as change of size and distribution of the sp^2 clusters during dry conditions

This study underlines the potential of DLC on thermoplastics to enhance the tribological performance. The tribological analysis in a rolling-sliding contact and subsequent Raman analysis are presented in future studies. Future work will focus on application of DLC coatings on gears made of polymers.

Acknowledgements The authors gratefully acknowledge the financial support of the German Research Foundation, Deutsche Forschungsgemeinschaft (DFG), within the project “Thermo-Elastohydrodynamics of Coated Polymer Gears” BO 1979/57-1 and STA 1198/8-1 in cooperation with Czech Science Foundation (GACR) 18-26849J. The authors would also like to acknowledge the support of the HLD at Helmholtz Zentrum Dresden-Rossendorf (HZDR), Dresden-Rossendorf, Germany, member of the European Magnetic Field Laboratory (EMFL).

Author Contributions KB: Conceptualization, Methodology, Resources, Writing—Review & Editing, Supervision, Project administration, Funding acquisition. CK: Conceptualization, Methodology, Writing—Review & Editing, Supervision, Project administration, Funding acquisition. MT: Conceptualization, Methodology, Investigation, Writing—Original Draft, Visualization. PŠ: Conceptualization, Methodology, Investigation, Writing—Contribution to Original Draft, Visualization. MH: Conceptualization, Methodology, Resources, Writing—Review & Editing, Supervision, Project administration, Funding acquisition. KS: Conceptualization, Methodology, Resources, Writing—Review & Editing, Supervision, Project administration, Funding acquisition. TL: Conceptualization, Methodology, Writing—Review & Editing, Supervision, Project administration, Funding acquisition. EM: Conceptualization, Methodology, Investigation, Writing—Review & Editing, Funding acquisition. SR: Conceptualization, Methodology, Investigation, Writing—Original Draft, Visualization.

Funding Open Access funding enabled and organized by Projekt DEAL. This study was funded by German Research Foundation, Deutsche Forschungsgemeinschaft (DFG), within the project “Thermo-Elastohydrodynamics of Coated Polymer Gears” BO 1979/57-1 and STA 1198/8-1 in cooperation with Czech Science Foundation (GACR) 18-26849 J.

Data Availability The data that support the findings of this study are available from the corresponding author upon reasonable request.

Code Availability Not applicable.

Declarations

Conflict of interest The authors declare that they have no known competing financial interests or personal relationships that could have appeared to influence the work reported in this paper.

Open Access This article is licensed under a Creative Commons Attribution 4.0 International License, which permits use, sharing, adaptation, distribution and reproduction in any medium or format, as long as you give appropriate credit to the original author(s) and the source, provide a link to the Creative Commons licence, and indicate if changes were made. The images or other third party material in this article are included in the article's Creative Commons licence, unless indicated otherwise in a credit line to the material. If material is not included in the article's Creative Commons licence and your intended use is not permitted by statutory regulation or exceeds the permitted use, you will need to obtain permission directly from the copyright holder. To view a copy of this licence, visit <http://creativecommons.org/licenses/by/4.0/>.

References

1. Domininghaus, H., Elsner, P., Eyrer, P., Hirth, T.: *Kunststoffe*. Springer, Berlin (2012)
2. Burris, D.L., Sawyer, W.G.: A low friction and ultra low wear rate PEEK/PTFE composite. *J. Tribol.* (2006). <https://doi.org/10.1016/j.wear.2005.12.016>
3. Davim, J.P., Cardoso, R.: Effect of the reinforcement (carbon or glass fibres) on friction and wear behaviour of the PEEK against steel surface at long dry sliding. *J. Tribol.* (2009). <https://doi.org/10.1016/j.wear.2008.11.003>
4. Friedrich, K., Karger-Kocsis, J., Lu, Z.: Effects of steel counterface roughness and temperature on the friction and wear of PE(E)K composites under dry sliding conditions. *J. Tribol.* (1991). [https://doi.org/10.1016/0043-1648\(91\)90287-5](https://doi.org/10.1016/0043-1648(91)90287-5)
5. Hanchi, J., Eiss, N.S.: Dry sliding friction and wear of short carbon-fiber-reinforced polyetheretherketone (PEEK) at elevated temperatures. *J. Tribol.* (1997). [https://doi.org/10.1016/S0043-1648\(96\)07347-4](https://doi.org/10.1016/S0043-1648(96)07347-4)
6. Lu, Z.P., Friedrich, K.: On sliding friction and wear of PEEK and its composites. *J. Tribol.* (1995). [https://doi.org/10.1016/0043-1648\(95\)90178-7](https://doi.org/10.1016/0043-1648(95)90178-7)
7. Schroeder, R., Torres, F.W., Binder, C., Klein, A.N., de Mello, J.: Failure mode in sliding wear of PEEK based composites. *J. Tribol.* (2013). <https://doi.org/10.1016/j.wear.2012.11.055>
8. Zhang, Z., Breidt, C., Chang, L., Friedrich, K.: Wear of PEEK composites related to their mechanical performances. *Tribol. Int.* (2004). <https://doi.org/10.1016/j.triboint.2003.09.005>
9. Rodriguez, V., Sukumaran, J., Schlarb, A.K., de Baets, P.: Reciprocating sliding wear behaviour of PEEK-based hybrid composites. *J. Tribol.* (2016). <https://doi.org/10.1016/j.wear.2016.05.024>
10. Theiler, G., Gradt, T.: Friction and wear of PEEK composites in vacuum environment. *J. Tribol.* (2010). <https://doi.org/10.1016/j.wear.2010.04.007>
11. Lhymn, C., Tempelmeyer, K.E., Davis, P.K.: The abrasive wear of short fibre composites. *Composites* (1985). [https://doi.org/10.1016/0010-4361\(85\)90619-6](https://doi.org/10.1016/0010-4361(85)90619-6)
12. Voss, H., Friedrich, K.: On the wear behaviour of short-fibre-reinforced peek composites. *J. Tribol.* (1987). [https://doi.org/10.1016/0043-1648\(87\)90262-6](https://doi.org/10.1016/0043-1648(87)90262-6)
13. Laux, K.A., Schwartz, C.J.: Effects of contact pressure, molecular weight, and supplier on the wear behavior and transfer film

- of polyetheretherketone (PEEK). *J. Tribol.* (2013). <https://doi.org/10.1016/j.wear.2012.11.013>
14. Zalaznik, M., Kalin, M., Novak, S.: Influence of the processing temperature on the tribological and mechanical properties of poly-ether-ether-ketone (PEEK) polymer. *Tribol. Int.* (2016). <https://doi.org/10.1016/j.triboint.2015.08.016>
 15. Lugscheider, E., Bärwulf, S., Riester, M., Hilgers, H.: Magnetron sputtered titanium nitride thin films on thermoplastic polymers. *Surf. Coat. Technol.* (1999). [https://doi.org/10.1016/S0257-8972\(99\)00157-7](https://doi.org/10.1016/S0257-8972(99)00157-7)
 16. Riester, M., Bärwulf, S., Lugscheider, E., Hilgers, H.: Composition of the interface region of sputtered titanium nitride thin films on thermoplastic polymers. *Surf. Coat. Technol.* (1999). [https://doi.org/10.1016/s0257-8972\(99\)00156-5](https://doi.org/10.1016/s0257-8972(99)00156-5)
 17. Lugscheider, E., Bobzin, K., Maes, M., Krämer, A.: On the coating of polymers—basic investigations. *Thin Solid Films* (2004). <https://doi.org/10.1016/j.tsf.2003.12.134>
 18. Bobzin, K., Bagcivan, N., Goebels, N.: PVD Beschichtung von Polyetheretherketon (PEEK) zur Verschleiß- und Reibungsminimierung im Kontakt Käfig-Führungsbord eines Spindellagers. *Tribol. Schmierungstech.* **2008**, 11–15 (2008)
 19. Karpinski, S., Salz, D., Paulkowski, D.: From steel to plastics friction reducing diamond-like carbon films, pp. 34–38. *Tribologie und Schmierungstechnik*, Germany (2016)
 20. Kaczorowski, W., Szymanski, W., Batory, D., Niedzielski, P.: Tribological properties and characterization of diamond like carbon coatings deposited by MW/RF and RF plasma-enhanced CVD method on poly(ether-ether-ketone). *Plasma Process. Polym.* (2014). <https://doi.org/10.1002/ppap.201400025>
 21. Dufils, J., Faverjon, F., Héau, C., Donnet, C., Benayoun, S., Valette, S.: Combination of laser surface texturing and DLC coating on PEEK for enhanced tribological properties. *Surf. Coat. Technol.* (2017). <https://doi.org/10.1016/j.surfcoat.2017.09.028>
 22. Bobzin, K., Brögelmann, T., Kalscheuer, C., Thiex, M.: Steigerung der Leistungsfähigkeit technischer Kunststoffe durch DLC-Beschichtungen. *Tribol. Schmierungstech.* **67**, 15–24 (2020)
 23. Kalish, R., Lifshitz, Y., Nugent, K., Prawer, S.: Thermal stability and relaxation in diamond-like-carbon. A Raman study of films with different sp³ fractions (ta-C to a-C). *Appl. Phys. Lett.* (1998). <https://doi.org/10.1063/1.123971>
 24. Ferrari, A.C., Robertson, J.: Raman spectroscopy of amorphous, nanostructured, diamond-like carbon, and nanodiamond. *Phil. Trans. R. Soc. A.* (2004). <https://doi.org/10.1098/rsta.2004.1452>
 25. Ferrari, A.C., Robertson, J.: Interpretation of Raman spectra of disordered and amorphous carbon. *Phys. Rev. B* (2000). <https://doi.org/10.1103/PhysRevB.61.14095>
 26. Casiraghi, C., Ferrari, A.C., Robertson, J.: Raman spectroscopy of hydrogenated amorphous carbons. *Phys. Rev. B* (2005). <https://doi.org/10.1103/PhysRevB.72.085401>
 27. Ferrari, A.C., Robertson, J.: Resonant Raman spectroscopy of disordered, amorphous, and diamondlike carbon. *Phys. Rev. B* **64**, 075414 (2001)
 28. Bobzin, K., Brögelmann, T., Kruppe, N.C.: Enhanced PVD process control by online substrate temperature measurement. *Surf. Coat. Technol.* (2018). <https://doi.org/10.1016/j.surfcoat.2018.07.096>
 29. Fischer-Cripps, A.C.: *Nanoindentation*. Springer eBook collection. Springer, New York (2004)
 30. Oliver, W.C., Pharr, G.M.: An improved technique for determining hardness and elastic modulus using load and displacement sensing indentation experiments. *J. Mater. Res.* (1992). <https://doi.org/10.1557/JMR.1992.1564>
 31. Bobzin, K., Brögelmann, T., Kruppe, N.C., Arghavani, M., Mayer, J., Weirich, T.E.: Plastic deformation behavior of nanostructured CrN/AlN multilayer coatings deposited by hybrid dcMS/HPPMS. *Surf. Coat. Technol.* (2017). <https://doi.org/10.1016/j.surfcoat.2017.06.092>
 32. Laukotka, E.: Referenzöle Datensammlung. FVA-Heft Nr., 660. Forschungsvereinigung Antriebstechnik e.V. (2007)
 33. Catena, A., Agnello, S., Cannas, M., Gelardi, F.M., Wehner, S., Fischer, C.B.: Evolution of the sp² content and revealed multilayer growth of amorphous hydrogenated carbon (a-C:H) films on selected thermoplastic materials. *Carbon* (2017). <https://doi.org/10.1016/j.carbon.2017.02.093>
 34. McC Ettlles, C.M.: Polymer and elastomer friction in the thermal control regime. *A S L E Trans.* (1987). <https://doi.org/10.1080/05698198708981743>

Publisher's Note Springer Nature remains neutral with regard to jurisdictional claims in published maps and institutional affiliations.